Superconductivity in Nb_4MSi (M=Ni, Co, and Fe) with a quasi-two-dimensional Nb network

Gihun Ryu,[1,*] Sung Wng Kim,[2] Satoru Matsuishi,[1] Hitoshi Kawaji,[1] and Hideo Hosono[1,2]

[1]*Materials and Structures Laboratory, Tokyo Institute of Technology, Mail Box S2-13, 4259 Nagatsuta-cho, Midori-ku, Yokohama 226-8503, Japan*

[2]*Frontier Research Center, Tokyo Institute of Technology, 4259 Nagatsuta-cho, Midori-ku, Yokohama 226-8503, Japan*

(Received 14 July 2011; revised manuscript received 4 December 2011; published 28 December 2011)

The $CuAl_2$-type Nb_4MSi (M = Ni, Co, and Fe) compound is composed of a quasi-two-dimensional Nb network. We found that Nb_4NiSi with a space group of $P4/mcc$ is a bulk type-II superconductor (lower critical field value of 10.7 mT and upper critical field value of 1.89 T), with the highest critical temperature (T_c of 7.7 K) among these compounds. The electron–phonon coupling constant of ~0.6 and Debye temperature of 415 K are estimated from the results of heat capacity measurements, and the density functional theory calculation indicates that the electronic density of states around the Fermi level is primarily composed of Nb 4d orbitals. We report the relationship between T_c and Debye temperature in the low-dimensional Nb-based system and attribute the relatively high T_c in Nb_4NiSi to the higher Debye temperature originating from the shortest Nb–Nb distance in the Nb network.

DOI: 10.1103/PhysRevB.84.224518 PACS number(s): 74.70.Ad, 74.90.+n, 74.25.−q, 81.05.Bx

I. INTRODUCTION

Compounds with a low-dimensional metal chain are interesting material systems with respect to several physical properties, including charge density wave (CDW) formation,[1–5] metal–insulator transition (MIT),[6,7] and emergence of superconductivity.[8–12] Among these properties, the superconductivity under a weak coupling regime of electron–phonon interactions ($\lambda_{el-ph} < 1$)[13,14] has attracted attention in the last several years due to correlations between the superconducting T_c and interchain interactions.[12] However, an understanding of the origin of superconductivity only using this relation in a low-dimensional system is insufficient.

An Nb-based compound with quasi-one-dimensional (quasi-1D) zigzag metal (Nb) chains appears to be suitable for investigating the superconductivity of low-dimensional systems. The superconductivity of these compounds has previously been reported for Nb_3Ch_4 (Ch = S, Se, and Te) with λ_{el-ph} of 0.51−0.59.[8,15] The Nb–Nb distance between intra- or interchains in this compound changes due to size variations of the Ch atoms, and T_c is influenced by two different factors: Nb–Nb distance and Debye temperature (Θ_D).[8,14,15] These observations indicate that Θ_D is crucial in order to understand the superconductivity of a low-dimensional Nb-based system.

To date, research on this low-dimensional system has been focused on Nb_3Ch_4 with a quasi-1D Nb topology, whereas Nb-based compounds with a quasi-two-dimensional (quasi-2D) Nb topology have not been studied. Thus, research on a quasi-2D Nb topology is necessary to understand the origin of superconductivity in this low-dimensional system. Nb_4MSi (M = Ni, Co, and Fe), which is composed of a quasi-2D Nb network, is a suitable model material for this purpose. Herein, we report the discovery of superconductivity at 7.7 K in Nb_4NiSi, which has the shortest Nb−Nb distance among Nb_4MSi compounds, and we discuss the primary factor controlling T_c in this low-dimensional Nb-based system.

II. EXPERIMENTAL METHODS

Polycrystalline samples of Nb_4MSi (M = Ni, Co, and Fe) were prepared by arc-melting a stoichiometric amount of high-purity niobium (99.9%, grain, Kojundo), nickel (cobalt and iron) (99.99%, grain, Kojundo), and silicon (99.995%, chip, Kojundo) under an argon gas atmosphere using a tungsten electrode and a water-cooled copper hearth. A 3 g ingot was arc-melted seven times from different sides to promote sample homogeneity. The ingots were subsequently annealed at 1373–1573 K for 96–144 h in evacuated silica tubes to remove the accumulated stress during arc-melting and then quenched. This postannealing procedure significantly affected the superconducting properties of Nb_4MSi compounds.

Crystalline phases of the resulting samples were identified by powder x-ray diffraction (PXRD) using a Bruker diffractometer model D8 ADVANCE (Mo rotating anode). Electrical resistivity measurements were performed using the conventional direct current (DC) four-probe method (Quantum Design Physical Property Measurement System: PPMS) between 2 and 300 K under a static magnetic field up to 2.4 T, whereas the DC magnetic susceptibility was measured between 2 and 13 K using PPMS with a Vibrating Sample Magnetometer (VSM) attachment. Specific heat measurements were performed by the thermal relaxation method in the temperature range of 1.8–15 K. To improve thermal contact, the annealed sample (14 mg) was mounted on a thin platform with Apiezon N grease, and the chemical composition of the sample was examined by electron probe microscope analysis (EPMA) with backscattered electron (BSE) mode. The electronic energy band structure and density of states (DOS) were calculated by the plane-wave total energy method using generalized gradient approximation (GGA) and Perdew-Burke-Ernzerhof (PBE) ultrasoft pseudopotentials implemented in CASTEP code.[16] To confirm the contribution of each atomic orbital to the electronic states near the Fermi level, the projected density of states (PDOS) was calculated for each atom.

III. RESULTS

A. Structural characterization

Figure 1(a) shows the PXRD pattern of annealed Nb_4NiSi as a representative compound of Nb_4MSi. Two kinds of space groups of $P4/mcc$ and $I4/mcm$ were previously reported for the crystal structure of $CuAl_2$-type Nb_4MSi compounds. The difference between these two space groups is due to the ordered or disordered state of M (M = Ni, Co, and Fe) and Si atoms.[17,18] The Ni and Si atoms are ordered in the superstructure of $P4/mcc$ with the position of Ni (0,0,1/4) and Si (1/2,1/2,1/4) and occupancy ratio of Ni/Si ∼1.00, whereas they are disordered in $I4/mcm$ with the position of Ni and Si (0,0,1/4) and occupancy ratio of Ni/Si ∼0.77. When fitting the PXRD pattern only with the space group of $P4/mcc$, the fitting was poor. For example, several diffraction peaks (16.33°, 16.81°, etc.) were not matched with the space group of $P4/mcc$. However, we could obtain better fitting by applying the two-phase model of the $I4/mcm$ space group. Thus, we concluded that the samples are mixtures of these two phases. The phase constitution obtained by Rietveld analysis is summarized in Table I. The main phase has the $P4/mcc$ space group and a volume fraction of 80%, and the phase with $I4/mcm$ has 10 vol.%. In addition, impurity phases identified are Nb_3Ni_2Si (∼2 vol.%),[19] $NbNi_3$ (∼5 vol.%),[20] Nb (∼3 vol.%),[21,22] and other small unknown Ni- or Si-rich phases.

Figure 1(b) shows the crystal structure of the Nb_4MSi compound described on the basis of Rietveld analysis. The Nb substructure in this compound is stretched to the direction of the (110) plane of the crystal structure, forming a graphite-like network composed of two different Nb−Nb distances of 2.78 and 2.99 Å.

Figures 1(c-1) and 1(c-2) show the BSE image in EPMA for the as-cast and postannealed Nb_4NiSi samples. The impurity phases such as the Nb-rich phase are conspicuously decreased, whereas the main phases ($P4/mcc$) of Nb_4MSi are increased through the postannealing process, as summarized in Table II. After the sample is annealed, however, unknown impurity phases still exist that have a deeper color than that of the Nb_4NiSi phase, as shown in element mapping images. The chemical composition of the main phase was 66.0, 17.3, and 16.7 at.% for Nb, Ni, and Si, respectively, and their values were close to the stoichiometry of $Nb_4Ni_1Si_1$. Moreover, the ratio of Ni/Si obtained by EPMA was ∼1.03, which agrees well with the result (Ni/Si = ∼1.00) obtained by Rietveld analysis. This small deviation in the composition is basically attributed to a short diffusion length of each element under the postannealing process.

B. Superconducting properties

Figure 2(a) depicts the electrical resistivity (ρ) as a function of temperature for Nb_4NiSi, the representative compound among Nb_4MSi. The onset of the superconducting transition temperature (T_c^{onset}) was ∼7.7 K, and zero resistivity occurred at 7.3 K. The ρ value decreased from 1.13×10^{-4} Ω·cm at 300 K as the temperature decreased, as shown in the inset of Fig. 2(a). Figure 2(b), which represents the DC magnetic susceptibility measurement, shows a large diamagnetic response below 7.7 K for both zero-field-cooling (ZFC) and field-cooling (FC) processes. The shielding volume fraction (SVF) evaluated from this slope was ∼42% at 2 K. These observations verify that Nb_4NiSi is a bulk superconductor with

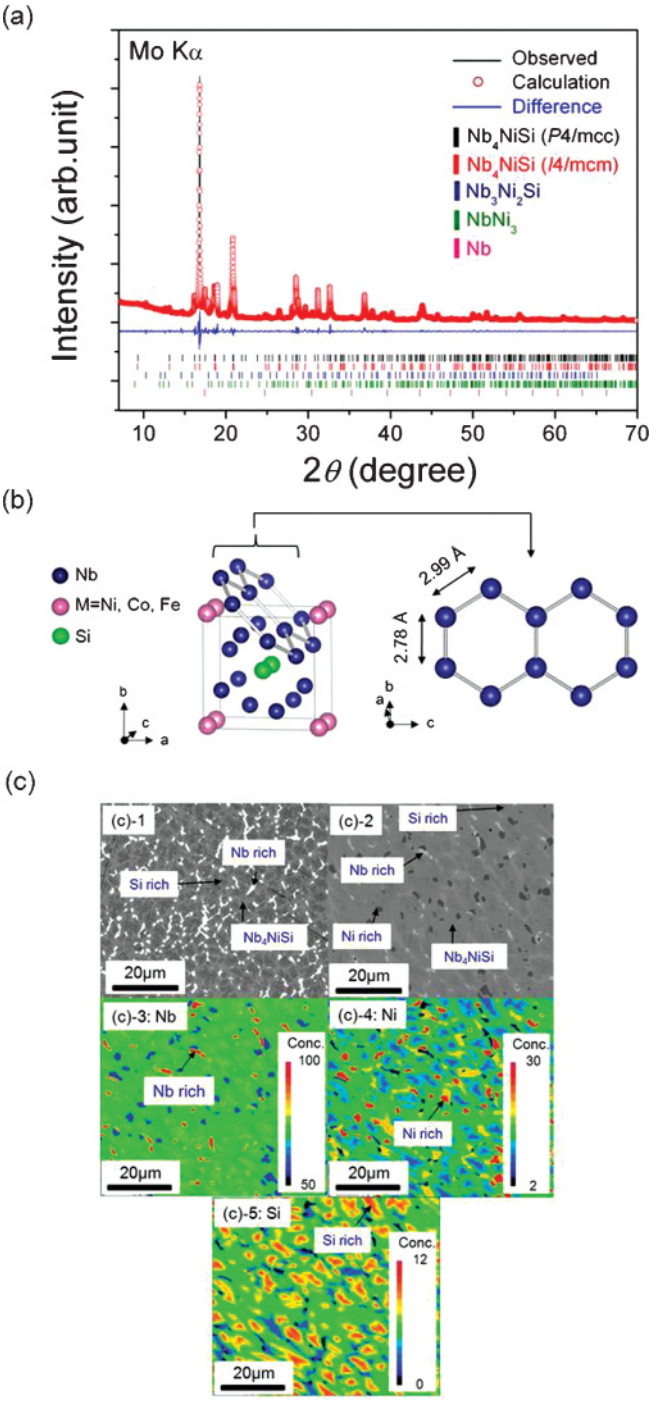

FIG. 1. (Color online) (a) Powder x-ray diffraction pattern (XRD) of the synthesized Nb_4NiSi sample (x-ray source: Mo Kα). Vertical bars represent the Bragg peaks for the structure with the space group of $P4/mcc$ mixed with $I4/mcm$. Peaks for the impurity phases are shown for comparison. (b) Left is the crystal structure of Nb_4MSi (M = Ni, Co, and Fe), where the solid line indicates a unit cell. Right is the structure of a quasi-2D Nb network in the (110) plane. (c) Backscattered electron image of as-cast (c-1) and postannealed (c-2) samples and element mapping for Nb (c-3), Ni (c-4), and Si (c-5) in the postannealed sample (c-2).

TABLE I. Crystal data and results of the structural refinements for Nb_4NiSi.

Formula	Nb_4NiSi	
Space group	$P4/mcc$ (No.124)	$I4/mcm$ (No.140)
Lattice parameters		
a (Å)	6.1948(1)	6.2003(2)
c (Å)	5.0390(2)	4.9952(2)
V (Å^3)	193.37(1)	192.03(1)
Z	2	4
R_p	4.97%	
R_{wp}	6.84%	
R_{exp}	1.94%	
Goodness of fit	3.52	
Atomic parameters		
Nb	8m (x, y, 0) $x = 0.1578(1)$, $y = 0.6594(1)$	8h (x, y, 0) $x = 0.1691(7)$, $y = 0.6416(8)$
Ni	2a(0,0,0.25)	4a(0,0,0.25)
Si	2c(0.5,0.5,0.25)	

$T_c = 7.7$ K, which originates from the phase of $P4/mcc$. This T_c is relatively higher than that of other Nb_4MSi (M = Co, Fe) compounds (Table II).

Figure 3(a) exhibits the magnetic field dependence of the magnetization of Nb_4NiSi measured at various temperatures to estimate the $H_{c1}(T)$. The inset of Fig. 3(a) shows $\mu_0 H_{c1}(T)$ as a function of $(T/T_c)^2$. The value of $\mu_0 H_{c1}(T)$ was fitted by the relation of the Ginzburg–Landau (GL) theory,[23] and $\mu_0 H_{c1}(0)$ was 10.9 ± 0.2 mT. Figure 3(b) shows the magnetic field dependence of the electrical resistivity between 2 and 10 K. T_c^{onset} shifted to the lower temperature as the magnetic field increased up to 2.4 T. The inset of Fig. 3(b) plots $\mu_0 H_{c2}$ as a function of temperature, and the empirical formula in Ginzburg–Landau (GL) theory[13] estimated $\mu_0 H_{c2}(0)$ as 1.89 ± 0.03 T. These results demonstrate that Nb_4NiSi is a type-II superconductor.

Figure 4 shows the heat capacity (C_p) of Nb_4NiSi below 13 K. The specific heat jump, which occurred at a temperature consistent with T_c values determined by resistivity and magnetic susceptibility measurements, confirmed the bulk nature of superconductivity. The critical temperature from specific heat data was defined as the midpoint of the transition $T_c^{mid,C}$ = 7.2 K. Below T_c, the C_p-T data followed an exponential decay. The normalized specific heat jump value $\Delta C/\gamma T_c^{mid,C}$ was 0.93 ± 0.01, which was substantially smaller than the

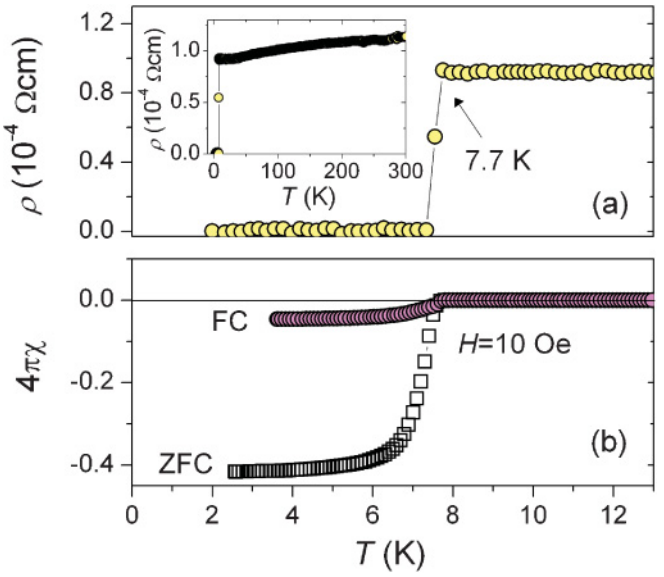

FIG. 2. (Color online) Temperature dependence of (a) zero-field resistivity and (b) magnetic susceptibility of Nb_4NiSi. Inset in (a) shows the resistivity throughout the entire temperature region.

mean-field BCS value of 1.43.[24] Because the specific heat in the normal state far below Θ_D is composed of electron and phonon contributions, C_p can be represented by[13]

$$C_p(T)/T = (C_{el} + C_{ph})/T = \gamma + \beta T^2, \quad (1)$$

where C_{el} and C_{ph} are the electronic and lattice specific heat, respectively, and γ and β are the coefficients for the electronic and phononic contributions. By the fitting the C_pT^{-1}–T^2 plot (the inset of Fig. 4), γ and β in the normal state were determined to be 14.1 ± 0.1 mJ mol^{-1} K^{-2} and 0.1615 ± 0.008 mJ mol^{-1} K^{-4}, respectively. The γ value would primarily come from Nb_4NiSi, because this value in other ternary metal alloys is not largely changed (<6%) by impurity.[25] It should be noted that most of phononic contribution (β) in Nb_4NiSi would also come from the lattice vibrations along the direction of stretched quasi-2D Nb network, similar to the $CuAl_2$ compound.[18] Since β can be expressed as[23]

$$\beta = 12\pi^4 nR/5\Theta_D^3, \quad (2)$$

where n is the number of atoms per formula unit for Nb_4NiSi, and R is the gas constant, Θ_D was evaluated as 415 ± 4 K. Θ_D can be related to the cutoff phonon frequencies through $k\Theta_D =$

TABLE II. Comparison of structural and superconducting parameters for Nb_4MSi (M = Ni, Co, and Fe).[a]

	As-cast sample					Postannealed sample				
	Phase fraction (vol.%)					Phase fraction (vol.%)				
	411 phase			T_c	SVF	411 phase			T_c	SVF
M	$P4/mcc$	$I4/mcm$	Nb	(K)	(%)	$P4/mcc$	$I4/mcm$	Nb	(K)	(%)
Ni	56	27	7	7.2	12	80	10	3	7.7	42
Co	80	15	5	4.1	7	84	13	2	6.0	7
Fe	79	2	10	5.0	12	84	2	8	6.8	78

[a]Lattice constant of postannealed samples in Nb_4MSi (M = Co and Fe); Co (a axis: 6.1637[2]Å, c axis: 5.0563[7] Å) and Fe (a axis: 6.1819[4] Å, c axis: 5.0364[2] Å).

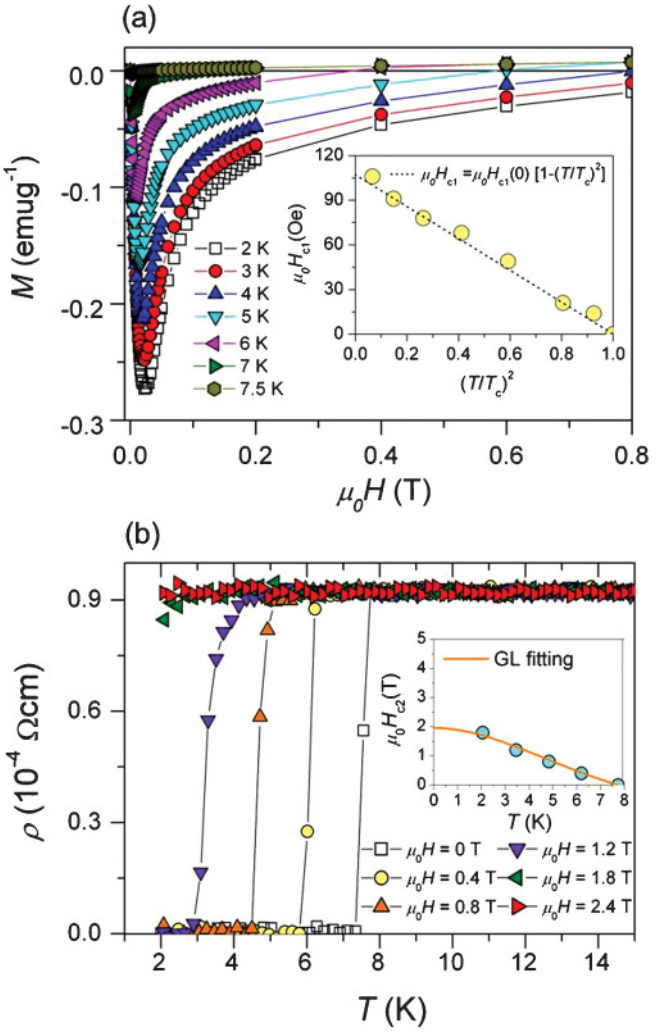

FIG. 3. (Color online) (a) Magnetic field dependence of magnetization (M–H curve) of Nb_4NiSi measured at various temperatures. Inset is the lower critical field, H_{c1}, as a function of $(T/T_c)^2$, used to estimate $\mu_0 H_{c1}(0)$. Dotted line is a linear fit for the relation of $\mu_0 H_{c1}(T) = \mu_0 H_{c1}(0)(1 - [T/T_c]^2)$. (b) ρ–T curve of Nb_4NiSi under various magnetic fields. Inset is a plot to estimate the upper critical field $\mu_0 H_{c2}(0)$. Curve indicates the fit to the Ginzburg–Landau (GL) expression.

$\hbar\omega_D$, where ω_D denotes the maximum phonon frequency, and k and $\hbar$ are the wave vector and Plank's constant, respectively.

The electron–phonon constant (λ_{el-ph}) was obtained by substituting the Θ_D value in McMillan's formula [Eq. (3)][13]

$$T_c = (\Theta_D/1.45)\exp[-1.04(1+\lambda_{el-ph})/\lambda_{el-ph} - \mu^*(1+0.62\lambda_{el-ph})], \quad (3)$$

where the Coulomb pseudopotential μ^* was assumed to be 0.1.[14] The obtained value of λ_{el-ph} was 0.60, and this small value implied that, similar to other Nb-based compounds such as Nb_3Ch_4,[14] Nb_4NiSi is classified as a weak-coupling superconductor.[13] The electronic density of states at the E_F was evaluated as $N(E_F) = 1.8$ state eV^{-1} f.u.$^{-1}$ using the formula $\gamma = (2/3)\pi^2 k^2_B(1+\lambda)N(E_F)$.

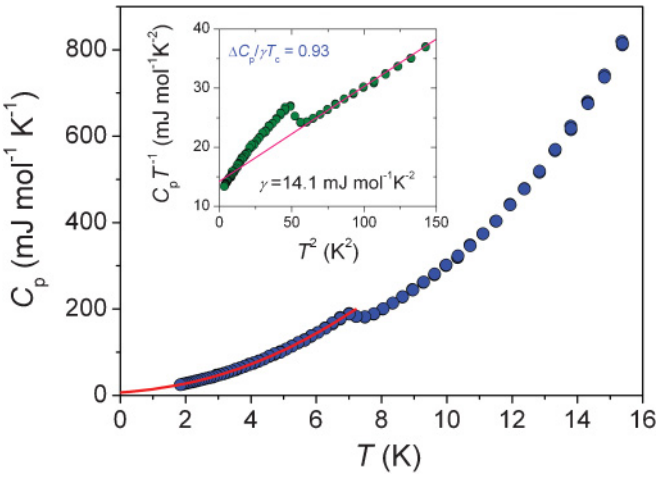

FIG. 4. (Color online) Temperature dependence of the specific heat for Nb_4NiSi. Inset plots $C_p T^{-1}$ vs T^2. Solid line shows the fit to the experimental data using the Debye formula (Eq. (1)).

IV. DISCUSSION

It is obvious from the results obtained from the Rietveld analysis of PXRD patterns of the annealed samples and SVF that the bulk superconductivity of $T_c = 7.7$ K originates from the main phase of Nb_4NiSi with $P4/mcc$. Among the Nb_4MSi compounds examined in the present study, Nb_4NiSi showed the highest T_c as summarized in Table II. So, we discuss Nb_4NiSi in the following section.

The Nb_4MSi (M = Ni, Co, and Fe) superconductor has a unique quasi-2D Nb network. As shown in Fig. 1(b), the Nb substructure seems to be a graphite-like 2D network. Polarized Raman spectra of the $CuAl_2$ compound as the prototype of Nb_4MSi may be understood by considering the 2D vibrations of the Al network.[18] From structural similarity, we consider that the isostructural Nb network in Nb_4MSi may be regarded as a quasi-2D network.

As shown in Fig. 5, the PDOS of Nb_4NiSi shows that the DOS around the Fermi level is mainly composed of Nb 4d

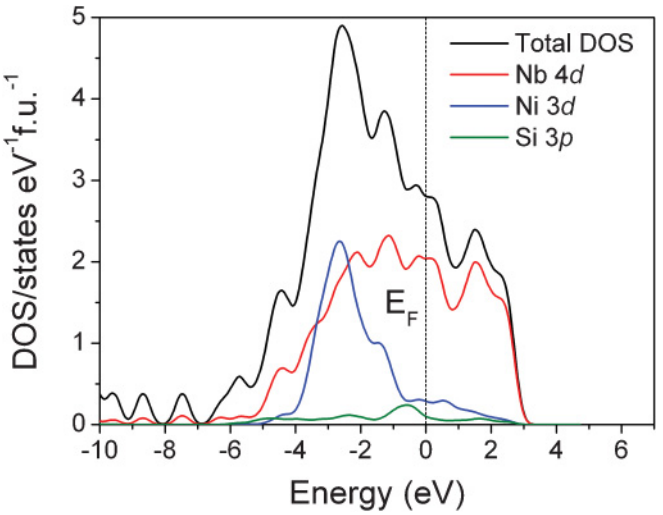

FIG. 5. (Color online) Total and projected density of states calculated for Nb_4NiSi with $P4/mcc$.

TABLE III. Comparison between structural and superconducting parameters among Nb-based compounds in a weak coupling regime.[a]

	Nb_4NiSi	Nb_3S_4	Nb_3Se_4	Nb_3Te_4
T_c (K)	7.7	3.7	2.3	1.9
Shortest Nb−Nb distance (Å)	2.779	2.881	2.885	2.973
γ [mJ mol^{-1} K^{-2}]	14.1 ± 0.1	13.6 ± 0.1	21.4 ± 0.2	18.7 ± 0.8
β [mJ mol^{-1} K^{-4}]	0.162 ± 0.008	0.328 ± 0.004	1.27 ± 0.02	11.40 ± 0.03
Θ_D	415 ± 4	346 ± 2	220 ± 2	106 ± 1
λ_{el-ph}	0.60	0.51	0.51	0.59
$N(E_F)$ [state eV^{-1} f.u.$^{-1}$]	1.8	1.9	3.0	2.5

[a]Data on Nb_3Ch_4 (Ch = S, Se, and Te) are compiled from Refs. 8, 14, 28, and 29.

orbitals. The $N(E_F)$ value obtained from the calculated DOS was 2.8 state eV^{-1} f.u.$^{-1}$ This value is comparable with that (1.8 state eV^{-1} f.u.$^{-1}$) estimated from experimentally obtained γ in C_p measurements. Similar to other Nb-based compounds such as Nb_3Ch_4 (Ch = S, Se, and Te) and $NbSe_3$,[26,27] this observation indicates that the metallic and superconducting transports mainly originate from Nb 4d electrons.

Next, we compare the presently studied Nb_4NiSi superconductor with other Nb-based superconductors composed of a low-dimensional Nb topology. These compounds belong to a weak electron–phonon coupling regime. On the basis of MacMillan formula [Eq. (3)] and $T_c = 1.13\Theta_D \exp(-1/VN[E_F])$,[13] where V is the electron–electron attractive interaction, we expect that T_c mainly depends on Θ_D, λ_{el-ph}, or $N(E_F)$. Table III summarizes the parameters associated with superconductivity and the structures of Nb-based compounds. Although λ_{el-ph} and $N(E_F)$ are almost independent of T_c, Θ_D is the dominant factor for T_c.

Interestingly, Nb_4MSi compounds follow the relationship between T_c and Θ_D as a function of Nb–Nb distance (Fig. 6). T_c gradually increases from Nb_3Te_4 with a quasi-1D Nb chain to Nb_4NiSi with a quasi-2D Nb network as the Nb–Nb distance decreases from 2.973 to 2.779 Å.[28,29] At the same time, Θ_D also increases with the decrease of the shortest Nb–Nb distance. In particular, this phononic contribution of C_p in Nb_4NiSi would probably be enhanced by the lattice vibration along the direction of the stretched quasi-2D Nb network similar to $CuAl_2$ compounds.[18] Otherwise, above a Nb–Nb distance of 3.038 Å, $NbCh_3$ with a 1D Nb chain does not exhibit superconductivity without the suppression of CDW.[8,9] From these results, it can be inferred that the evolution of T_c in a low-dimensional Nb-based system originates mostly from Θ_D of the Nb lattice.

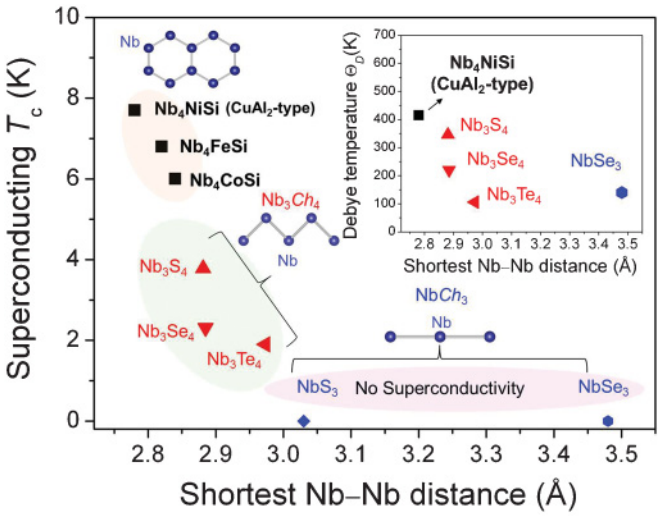

FIG. 6. (Color online) Superconducting critical temperature T_c as a function of the shortest Nb–Nb distance in Nb_4MSi (M = Ni, Co, Fe), Nb_3Ch_4 (Ch = S, Se, Te) per Refs. 8, 14, 28,29 and $NbCh_3$ (Ch = S, Se) per Refs. 30, 35, 36,37. Inset plots the Debye temperature (Θ_D) and shortest Nb–Nb distance.

It should be noted that these comparisons in a low-dimensional Nb-based system have been conducted in a weak electron–phonon coupling regime (see λ_{el-ph} in Table III). For a strong coupling regime, the relationship between T_c and Θ_D conversely changes. For example, T_c of A15-type compounds with a 1D Nb chain increases as Θ_D decreases.[30,31] Unlike a weak coupling regime, the softening of the Nb lattice significantly contributes to the enhancement of T_c.[31,32]

Finally, we would like to discuss the difference between Nb-based superconductors in terms of Nb topology. A pure Nb superconductor with a three-dimensional (3D) Nb lattice has a longer Nb–Nb distance (2.857 Å)[32] than that of Nb_4NiSi with a quasi-2 Nb network, and it exhibits a relatively strong λ_{el-ph} (∼1) but has a small Θ_D (∼277 K).[13] These values drastically differ from those of Nb_4NiSi (Θ_D ∼415 K, λ_{el-ph} ∼0.60), indicating that T_c of pure Nb is controlled by strong λ_{el-ph}, where the phonon of the Nb lattice is substantially softened by the interatomic charge–charge interactions in the 3D Nb lattice structure.[13,33,34]

V. CONCLUSIONS

$CuAl_2$-type Nb_4MSi (M = Ni, Co, and Fe) compounds with a quasi-2D Nb network exhibit superconductivity with T_c of 6.0–7.7 K. Among these compounds, the highest T_c of 7.7 K was observed in the Nb_4NiSi compound, and the relatively higher T_c in a low-dimensional Nb-based system is attributed to the higher Θ_D originating from a quasi-2D Nb lattice, and the Θ_D increases as the Nb–Nb distance decreases. We expect a higher T_c would be realized in Nb-based compounds with shorter Nb–Nb bonds.

ACKNOWLEDGMENTS

This work was supported by the Funding Program for World-Leading Innovative R and D on Science and Technology (FIRST), Japan.

*gh-ryu@lucid.msl.titech.ac.jp

[1]F. W. Boswell, A. Prodan, and J. M. Brandont, J. Phys. Solid State Phys. **16**, 1067 (1983).
[2]A. J. Berlinsky, Obst. Rep. Prog. Phys. **42**, 1233 (1979).
[3]K. Kawabata, J. Phys. Soc. Jpn. **54**, 762 (1985).
[4]T. Sekine, Y. Kiuchi, E. Matsuura, K. Uchinokura, and R. Yoshizaki, Phys. Rev. B **36**, 3153 (1987).
[5]Y. Ishihara and I. Nakada, Solid State Commun. **45**, 129 (1983).
[6]E. M. Dizhur, M. A. Il'ina, and V. Zaitsev-Zotov, JETP Lett. **86**, 132 (2007).
[7]V. Eyert, Europhys. Lett. **58**, 851 (2002).
[8]E. Amberger, K. Polborn, P. Grimm, M. Dietrich, and B. Obst, Solid State Commun. **26**, 943 (1978).
[9]P. Monceau, J. Peyrard, J. Richard, and P. Molinie, Phys. Rev. Lett. **39**, 161 (1977).
[10]W. Scherer, C. Hauf, M. L. Presnitz, E. W. Scheidt, G. Eickerling, V. Eyert, R. D. Hoffmann, U. C. Rodewald, A. Hammerschmidt, C. Vogt, and R. Pttgen, Angew. Chem. Int. Ed. **49**, 1578 (2010).
[11]J. C. Armici, M. Decroux, Q. Fischer, M. Potel, R. Chevrel, and M. Sergent, Solid State Commun. **33**, 607 (1980).
[12]B. Horovitz and A. Birnboim, Solid State Commun. **19**, 91 (1976).
[13]C. P. Poole Jr., H. A. Farach, R. J. Creswick, and R. Prozov, *Superconductivity*, 2nd ed. (Academic Press, New York, 2007); W. L. McMillan, Phys. Rev. **167**, 331 (1968).
[14]H. Okamoto, H. Taniguti, and Y. Ishihara, Phys. Rev. B **53**, 384 (1996).
[15]T. Dobashi, T. Sato, S. Souma, T. Takahashi, H. Kaneko, Y. Ishihara, and H. Okamoto, Phys. Rev. B **76**, 045121(2007).
[16]J. P. Perdew, K. Burke, and M. Ernzerhof, Phys. Rev. Lett. **77**, 3865 (1996).
[17]E. I. Gladyshevski and Y. B. Kuzma, Z. Strukt. Khim. **6**, 60 (1963).
[18]Y. Grin, F. R. Waner, M. Armbruster, M. Kohout, A. Leithe-Jasper, U. Schwarz, U. Wedig, and H. Georg von Schering, J. Solid State Chem. **179**, 1707 (2006).
[19]E. I. Gladyshevskii, Y. B. Kuz'ma, and P. I. Kripyakevich, Z. Strukt. Khim. **4**, 372 (1963).
[20]A. Brauner, C. A. Nunes, A. D. Bortolozo, G. Rodrigues, and A. J. S. Machado, Solid State Commun. **54**, 899 (1989).
[21]A. G. Knapton, Nature **175**, 730 (1955).
[22]E. I. Gladyshevski, Y. B. Kuzma, and P. I. Kripyakevich, Z. Strukt. Khim. **4**, 372 (1963).
[23]K. Kawashima, M. Maruyama, M. Fukuma, and J. Akimitsu, Phys. Rev. B **82**, 094517 (2010).
[24]J. Bardeen, L. N. Cooper, and J. R. Schriefffer, Phys. Rev. **108**, 1175 (1957).
[25]T. H. Davis and J. A. Rayne, Phys. Rev. B **6**, 2931 (1972).
[26]A. Oshiyama, J. Phys. Soc. J. **52**, 587 (1983).
[27]R. Hoffmann, S. Shaik, J. C. Scott, M. H. Whangbo, and M. J. Foshee, J. Solid State Chem. **34**, 263 (1980).
[28]A. F. Ruysink, F. Kadijk, A. J. Wagner, and F. Jellinek, Acta Crystallogr. **24**, 1614 (1968).
[29]K. Selte and A. Kjekshus, Acta Crystallogr. **17**, 1568 (1964).
[30]K. E. Kihlstrom, D. Mael, and T. H. Geballe, Phys. Rev. **29**, 150 (1984).
[31]J. Kwo and T. H. Geballe, Phys. Rev. B **23**, 3230 (1981).
[32]A. Pialoux, M. L. Joyeux, and G. Cizeron, J. Less-Common Metals **87**, 1 (1982).
[33]L. F. Mattheiss, Phys. Rev. B **1**, 373 (1970).
[34]P. B. Allen, Phys. Rev. B **16**, 5139 (1977).
[35]J. L. Hodeau, M. Marezio, C. Roucau, R. Ayroles, A. Meerschaut, J. Rouxel, and P. Monceau, J. Phys. C **11**, 4117 (1978).
[36]E. Dizhur, M. Il'ina, and S. Zaitzev-Zotov, Phys. Status Solidi B **246**, 500 (2009).
[37]J. C. Lasjaunias and P. Monceau, Solid State Commun. **41**, 911 (1982).